TIGIT Affects CAR NK-cell Effector Function in the Solid Tumor Microenvironment by Modulating Immune Synapse Strength

Ishwar Navin[1], Matthew Dysthe[2], Prashant S. Menon[3], Corrine Baumgartner[4], Tim Sauer[5], Navin Varadarajan[3], and Robin Parihar[1,4,6]

ABSTRACT

Therapies using NK cells that express chimeric antigen receptors (CAR-NK) have been successfully employed against hematologic malignancies. However, solid tumors resist CAR-NKs partly by enriching tumor microenvironments with ligands for NK cell inhibitory receptors. Although the NK inhibitory receptor T-cell immunoreceptor with immunoglobulin and immunoreceptor tyrosine-based inhibitory motif domain (TIGIT) has been implicated in impaired antitumor activity of endogenous NK cells, the consequences of TIGIT expression on engineered CAR-NKs have not been explored. To address this gap, we compared TIGIT-expressing and TIGIT-deleted human CAR-NKs targeting the GD2 solid tumor antigen in tumor immune microenvironment cocultures and *in vivo* tumor immune microenvironment xenografts designed to mimic the immunosuppressive environment of solid tumors. TIGIT-deleted GD2.CAR-NKs exhibited antitumor activity, expanded, and persisted within TIGIT ligand–enriched solid tumor environments, whereas TIGIT-expressing CAR-NKs did not. Mechanistic experiments revealed that the improved tumor control resulting from TIGIT loss on CAR-NKs was not dependent on DNAM-1 activation or enhanced cytotoxic potential but rather on downregulation of cell adhesion molecules, weakened cell avidity, and reduced synapse contact duration that, in concert, improved serial killing and allowed more efficient tumor destruction. Our study highlights a noncanonical role for TIGIT in modulating CAR-NK activity that may guide strategies to overcome inhibitory NK receptors like TIGIT and improve the efficacy of CAR-NKs against solid tumors.

Introduction

NK cells are cytotoxic lymphocytes of the innate immune system. Their cytotoxicity against target cells is governed by a balance of signals from germline-encoded activating and inhibitory receptors expressed on the NK cell surface (1). In contrast to adoptive T cell–based therapies for cancer, adoptive transfer of allogeneic NK cells does not result in GVHD or cytokine release syndrome (2, 3). In fact, therapy with allogeneic NK cells engineered to express a CD19-targeting chimeric antigen receptor (CAR) and IL15 resulted in improved outcomes in patients with relapsed or refractory B-cell malignancies without mediating the typical CAR-driven toxicities seen with T cells (4, 5). Although CAR-expressing NK cells (CAR-NK) have been successful in hematologic malignancies, their efficacy has been limited against solid tumors. This is partly due to a highly suppressive solid tumor immune microenvironment (TiME) that includes inhibitory myeloid cells such as M2 tumor-associated macrophages (M2-TAM) and myeloid-derived suppressor cells (MDSC) which express ligands against inhibitory receptors on infiltrating NK cells resulting in decreased effector function (6).

T-cell immunoreceptor with immunoglobulin and immunoreceptor tyrosine-based inhibitory motif domain (TIGIT) is an inhibitory receptor on NK cells and T cells, the ligands of which are upregulated in multiple solid tumors (7–9). TIGIT mediates its suppressive effect on NK cells by binding to its most abundant ligands, CD155 and CD112, overexpressed on malignant cells as well as M2-TAMs and MDSCs. This triggers inhibitory signaling in NK cells through TIGIT's intracellular immunoreceptor tyrosine-based inhibitory motif and immunoglobulin tail tyrosine-like domains (10). Given that TIGIT impairs cytotoxicity by endogenous NK cells and its overexpression is correlated with poor prognosis in patients with solid tumors (7, 11, 12), the TIGIT–ligand axis likely represents a powerful barrier to CAR-NK efficacy within solid TiMEs. Although the role of TIGIT in endogenous solid tumor–infiltrated NK cell activity has been studied, its effect on the behavior of CAR-NKs in these environments has not been reported. Addressing this gap in knowledge is clinically relevant as understanding mechanisms by which TIGIT impairs CAR-NK functions would allow the design of biology-driven strategies to overcome TIGIT inhibition and improve the efficacy of CAR-NK products designed for solid tumor anticancer therapy.

To interrogate the effect of persistent TIGIT engagement on CAR-NK antitumor responses specifically within the TiME, we compared a solid tumor–targeting CAR-NK with efficient and stable TIGIT knockout with TIGIT-expressing CAR-NKs in a TiME coculture and an *in vivo* TiME xenograft model designed to mimic the immunosuppressive environment of solid tumors. We show herein

[1]Department of Immunology and Microbiology, Baylor College of Medicine, Houston, Texas. [2]Department of Translational Biology and Molecular Medicine, Baylor College of Medicine, Houston, Texas. [3]William A. Brookshire Department of Chemical and Biomolecular Engineering, University of Houston, Houston, Texas. [4]Department of Pediatrics, Division of Hematology-Oncology, Baylor College of Medicine, Houston, Texas. [5]Department of Medicine V, Hematology, Oncology and Rheumatology, University Hospital Heidelberg, Heidelberg, Germany. [6]Center for Cell and Gene Therapy, Baylor College of Medicine, Houston Methodist, and Texas Children's Hospital, Houston, Texas.

Corresponding Author: Robin Parihar, Department of Pediatrics, Division of Hematology-Oncology, Baylor College of Medicine, Center for Cell and Gene Therapy, 1102 Bates Street, Suite 1770, Houston, TX 77030. E-mail: rxpariha@texaschildrens.org

Cancer Immunol Res 2025;XX:XX–XX

doi: 10.1158/2326-6066.CIR-24-0919

that TIGIT deletion enhanced CAR-NK proliferation and serial killing, conferring tumor control that extended the survival of mice bearing TiME xenografts. The enhanced CAR-NK functionality was not due to improvements in canonical signaling pathways normally inhibited by TIGIT, but instead, to a role for TIGIT in modulating immune synapse strength in CAR-NKs upon engagement with tumor targets. Our findings reveal a role for TIGIT in affecting antitumor function in CAR-NKs with implications in redefining the conventional thinking on the role of endogenous inhibitory receptors in lymphocytes engineered to express CARs.

Materials and Methods

Cytokines and cell lines

Recombinant human IL2 was obtained from National Cancer Institute Biologic Resources Branch (Frederick, MD). Recombinant human IL4 (200-04-100UG), IL6 (200-06-100UG), macrophage colony-stimulating factor (M-CSF; 300-25-100UG), GM-CSF (300-03-100UG), and IL15 (200-15-100UG) were purchased from PeproTech (Rocky Hill, NJ, USA). The human neuroblastoma cell lines CHLA255 (RRID: CVCL_AQ27, obtained 2021) and LA-N-1 (RRID: CVCL_1827, obtained 2017) were purchased from ATCC (Manassas, VA, USA) and cultured in RPMI-1640 culture medium (HyClone SH30096.01) supplemented with 2 mmol/L L-glutamine (Gibco-BRL, Cat. #35050061) and 10% FBS (Gibco-BRL, Cat. #A5670701). The human lung cancer cell line H1650 (RRID: CVCL_1483, obtained in 2024) was purchased from ATCC and cultured in complete DMEM culture medium composed of DMEM (HyClone, Cat. #SH30285.01) supplemented with 2 mmol/L L-glutamine and 10% FBS. The human CML cell line K562 (RRID: CVCL_0004, obtained in 2011) was purchased from ATCC and cultured in complete RPMI culture medium composed of RPMI-1640 medium (HyClone) supplemented with 2 mmol/L L-glutamine and 10% FBS. A modified version of parental K562 cells, genetically modified to express a membrane-bound version of IL15 and 41BB-ligand, K562-mb15-41BB-L, was kindly provided by Dr. Dario Campana (National University of Singapore), obtained in 2011. A modified version of parental K562, genetically modified to express CD80, CD86, and 41BB-L, K562-mb15-CS, was kindly provided by Dr. Cliona Rooney (Baylor College of Medicine) obtained in 2020. The human epithelial cell line HEK293T (RRID: CVCL_0063) purchased from ATCC (Manassas, VA, USA) and cultured in DMEM culture medium supplemented with 2 mmol/L L-glutamine (Gibco-BRL) and 10% FBS (Gibco-BRL), obtained in 2015. All cell lines were verified by either genetic or flow cytometry–based methods and tested for *Mycoplasma* contamination monthly via MycoAlert (Lonza, Cat. #LT07-318) Mycoplasma Enzyme Detection Kit. All cell lines were used within 1 month of thawing from early-passage (<3 passages of original vial) lots.

CAR-encoding retroviral vectors

The construction of the SFG-retroviral vector encoding GD2.CAR.41BB.ζ, as shown in Supplementary Fig. S1A, was previously described (13, 14). The HER2-specific single-chain variable fragment (FRP5)–based CAR transgenes were described previously (15). RD114-pseudotyped viral particles were produced by transient transfection in 293T cells, as previously described (16).

Antibodies and flow cytometry

The following antibodies were used in this study: CD56 (BD Biosciences, Cat. #555516, RRID: AB_395906), CD3 (BD Biosciences, Cat. #345763, RRID: AB_2811220; BioLegend, Cat. #344834, RRID: AB_2565675), TIGIT (BioLegend, Cat. #372706, RRID: AB_2632732; BioLegend, Cat. #372710, RRID: AB_2632925), NKp46 (BioLegend, Cat. #331916, RRID: AB_2561621, BioLegend, Cat. #331930, RRID: AB_2566117), CD16 (BioLegend, Cat. #302038, RRID: AB_2561578; BD Biosciences, Cat. #555407, RRID: AB_395807), DNAM-1 (BioLegend, Cat. #338316, RRID: AB_2616645), NKG2D (BioLegend, Cat. #320816, RRID: AB_2562747), NKG2A (BioLegend, Cat. #375120, RRID: AB_2888868), PD-1 (BioLegend, Cat. #329938, RRID: AB_2563596), TIM-3 (BioLegend, Cat. #345026, RRID: AB_2565717), LAG-3 (BioLegend, Cat. #369314, RRID: AB_2629797), CD45 (BioLegend, Cat. #368532, RRID: AB_2715892), GD2 (BioLegend, Cat. #357304, RRID: AB_2561885), CD155 (BioLegend, Cat. #337618, RRID: AB_2565815), CD112 (BioLegend, Cat. #337414, RRID: AB_2565732), CD33 (BD Biosciences, Cat. #555450, RRID: AB_395843), CD83 (BD Biosciences, Cat. #556910, RRID: AB_396534), HLA-DR (BD Biosciences, Cat. #347364, RRID: AB_400292), CD14 (BioLegend, Cat. #367144, RRID: AB_2810580), CD163 (BioLegend, Cat. #333622, RRID: AB_2563612), CD20 (BD Biosciences, Cat. #555622, RRID: AB_395988), CD107a (BioLegend, Cat. #328630, RRID: AB_2562109), Fas ligand (Fas-L; BioLegend, Cat. #306412, RRID: AB_2716105), IFNγ (BioLegend, Cat. #506538, RRID: AB_2801098), p-mTOR (Ser2448; Thermo Fisher Scientific Cat. #25-9718-42, RRID: AB_2573550), anti-CD247 (pY142; BD Biosciences, Cat. #558486, RRID: AB_647104), annexin V (BioLegend, Cat. #640950), 7-AAD (BD Biosciences, Cat. #559925, RRID: AB_2869266), FVS620 (BD Biosciences, Cat. #564996, RRID: AB_2869636), and FVS780 (BD Biosciences, Cat. #565388, RRID: AB_2869673). The GD2.CAR was detected using Alexa Fluor 647–conjugated 1A7 idiotypic antibody and FRP5 antibody (17, 18), or 1A7 idiotypic antibody followed by Rat anti–mouse IgG1 (BD Biosciences, Cat. #340270, RRID: AB_400010). Cells were stained with antibody for 15 minutes at 4°C. Samples were fixed using BD Cytofix Fixation Buffer. All samples were acquired on a Gallios Flow Cytometer (Beckman Coulter) or FACSCanto II (BD Biosciences), and data were analyzed using FlowJo analysis Software v11 (BD Biosciences, RRID: SCR_008520).

Intracellular staining

NK cells were fixed (BD Phosflow Fix Buffer I, BD Biosciences, Cat. #557870, RRID: AB_2869102), washed (BD Phosflow Perm/Wash I, BD Biosciences, Cat. #557885, RRID: AB_2869104), permeabilized with prechilled 100% methanol (BD Phosflow Perm Buffer II, BD Biosciences, Cat. #558052, RRID: AB_2869119) for 20 minutes on ice, and then washed twice. For phospho-FACS, cells were stained with either p-mTOR (Ser2448) or anti-CD247 (pY142) for 30 minutes at room temperature in the dark. For intracellular cytokine staining, NK cells were fixed, washed, permeabilized (eBioscience Foxp3/Transcription Factor Staining Buffer Set, eBioscience, Cat. #00-5523-00), and stained with anti-IFNγ for 30 minutes in the dark at 4°C. For viability, cells were stained with either 7-AAD, FVS620, or FVS780.

Expansion of human NK cells

Whole peripheral blood mononuclear cells (PBMC) or CD3-depleted PBMCs (Human CD3 Positive Selection Kit II, STEMCELL Technologies, Cat. #17851), obtained from 10 healthy blood donors consented under Baylor College of Medicine Institutional Review Board–approved protocols, were co-cultured with irradiated (100 Gy) K562-mb15-41BB-L in a 1:10 (NK cell:irradiated tumor cell) ratio in G-Rex cell culture devices (Wilson Wolf, St. Paul,

MN, USA Cat. #80040S) for 6 days in Stem Cell Growth Medium (CellGenix, Cat. #20802-0500) supplemented with 10% FBS and 500 IU/mL IL2. For some experiments that did not require further genetic engineering, NK cells were expanded for 7 days with either K562-mb15-41BB-L or K562-41BB-CS or pre-activated with IL12 (10 ng/mL), IL15 (50 ng/mL), and IL18 (50 ng/mL) for 16 hours followed by IL15 (10 ng/mL) for 6 days.

Guide RNA design

Guide RNAs (gRNA) targeting *TIGIT* were designed using the webtool (https://www.crisprscan.org/). Both TIGIT gRNAs utilized in the study target exon 2 (5′-TAATACGACTCACTATAGGTGACCGTGAACGATACAGGTTTTAGAGCTAGAA-3′) and (5′-TAATACGACTCACTATAGGGGGCCACTCGATCCTTGAGTTTTAGAGCTAGAA-3′). The *DNAM-1* gRNA (5′-TAATACGACTCACTATAGGTCTTCTTCATGTATACAGGTTTTAGAGCTAGAA-3′) was based on a design previously described (19). Conditions containing Cas9 without any scrambled gRNA were used as a negative control.

CRISPR-mediated gene deletion and retroviral transduction of human expanded NK cells

Cell suspensions on day 6 were harvested, and 3 to 4 × 10^6 NK cells were electroporated with Alt-R S.p. Cas9 Nuclease V3 (2 μg; IDT, Cat. #1081059), gRNAs (1 μg/gRNA), and 1 μL of Alt-R Cas9 Electroporation Enhancer (IDT, Cat. #10007805) in an electroporation strip (P3 Primary Cell 4D-Nucleofector X Kit S, Cat. #V4XP-3032) using the program DN-100 on the Lonza 4D-Nucleofector system. The protocol was adapted from a previously described article (20). Immediately after electroporation, NK cells were transduced with SFG-based retroviral vectors, as previously described (13) for 4 days in Stem Cell Growth Medium. $TIGIT^{KO}$ efficiency was validated using FACSCanto II (BD Biosciences) and ImageStream analysis by ImageJ v1.54k. Data were analyzed using FlowJo analysis software v11 (BD Biosciences). For *in vivo* experiments, the transduced cell population was subjected to secondary expansion to generate adequate cell numbers in G-Rex devices at a 1:1 (NK cell:irradiated K562-mb15-41BB-L cell) ratio with 100 IU/mL IL-2 for 7 days in complete Stem Cell Growth Medium.

Induction of human MDSCs and M2-TAMs *ex vivo*

$CD14^+$ PBMCs autologous to CD3-depleted PBMCs used for NK cell expansions were first isolated from healthy blood donors using magnetic column selection (Miltenyi Biotec) and incubated on 24-well tissue culture plates for 7 days with a GM-CSF (20 ng/mL) and IL6 (20 ng/mL) cytokine cocktail known to induce MDSCs, as previously described (21). M2 macrophages were generated from a similar starting $CD14^+$ PBMC material using M-CSF (100 ng/mL) and IL4 (20 ng/mL).

Degranulation and IFNγ assay

NK cells were co-cultured with GFP-tagged LA-N-1 neuroblastoma and *ex vivo* generated MDSCs at a 1:4:8 (NK cell:MDSC:tumor) ratio in a 24-well plate for 24 hours at 37°C. Anti-CD107a was added directly to the triculture at 20 hours. The protein transport inhibitor Brefeldin A (BioLegend, Cat. #420601) was added at 21 hours to the triculture and incubated for 3 hours at 37°C. Intracellular IFNγ and CD107a were analyzed using flow cytometry after the conclusion of the assay.

Tumor cytotoxicity kinetics assay

Unmodified, $TIGIT^{KO}$, GD2.CAR-NK, and $TIGIT^{KO}$GD2.CAR-NK cells labeled with a fluorescent dye (CellTracker Red CMTPX Dye, Invitrogen, Cat. #C34552) were incubated with GFP-CHLA255 neuroblastoma or GFP-H1650 lung carcinoma at 37°C in either a 4:1 or 1:4 and 1:20 NK cell:tumor ratio, respectively, for 96 hours on a 24-well tissue culture plate. Kinetic live-cell imaging cytotoxicity assays were conducted on an Incucyte S3 Live Cell Analysis System (Sartorius). Tumor cell growth was determined by measuring green object area per well.

Generation of an M2-TAM containing TiME culture

PBMC-derived $CD14^+$ monocytes and GFP-expressing CHLA255 neuroblastoma or H1650 lung carcinoma were incubated at a 1:1 monocyte:tumor ratio in a 24-well tissue culture plate for 72 hours at 37°C with 100 ng/mL M-CSF to promote monocyte survival. After 72 hours, a monolayer containing CHLA255 or H1650 admixed with tumor-induced M2-TAMs was established, and TiME properties such as inhibitory cytokine milieu, M2-TAM phenotype, and lymphocyte suppression were confirmed using multiplex ELISA of culture supernatants, M2-TAM flow cytometry, and Incucyte assay, respectively. After 72 hours, half of the media in each well was replaced with fresh complete RPMI to maintain viability of TiME in the cultures. Kinetic live-cell imaging cytotoxicity assays were conducted on an Incucyte S3 Live Cell Analysis System (Sartorius). Tumor cell growth was determined by measuring green object area per well.

TiME tumor cytotoxicity assay

After TiME establishment described above, 1 × 10^5 of fluorescently dye-labeled (CellTracker Red CMTPX Dye, Invitrogen) unmodified, $TIGIT^{KO}$, GD2.CAR-NK, and $TIGIT^{KO}$GD2.CAR-NK, DNAM-1^{KO}GD2.CAR-NK, and $TIGIT^{KO}$DNAM-1^{KO}GD2.CAR-NK cells were added to each well with 10 ng/mL IL15 and incubated at 37°C for 96 hours on the 24-well tissue culture plate. Kinetic live-cell imaging cytotoxicity assays were conducted on an Incucyte S3 Live Cell Analysis System (Sartorius). In some experiments, all NK cells were incubated for 72 hours at 37°C prior to being transferred to a new freshly prepared TiME. This step was repeated one more time. After every transfer, 10 ng/mL IL15 was provided to maintain NK survival. The green object area reading when NK cells are added to a prepared TiME (0 hour) is "green object area (T0)." The green object area reading after 72 hours of NK-TiME co-culture is "green object area (T72).". Therefore, the fold change in tumor burden is calculated as follows:

$$Fold\,Change(Tumor\,Burden) = \frac{Green\,Object\,Area\,(T72)}{Green\,Object\,Area\,(T0)}$$

In vivo TiME xenograft model

Six to 8-week-old male and female NSG-SGM3 mice (The Jackson Laboratory, Strain #013062, RRID: IMSR_JAX:013062) were implanted subcutaneously in the dorsal right flank with 1 × 10^6 LA-N-1 neuroblastoma cells admixed with 5 × 10^5 $CD14^+$ PBMCs, suspended in basement membrane Matrigel (Corning). LA-N-1 neuroblastoma cells do not express ligands for the most highly expressed NK activating receptor, NKG2D, but express GD2 and both TIGIT ligands at comparable levels with CHLA255 neuroblastoma (but which also has high levels of NKG2D ligands). This allows control for other NK activating receptors while isolating the effect of either TIGIT presence or absence on CAR-mediated effects. The Matrigel basement

membrane was important in keeping tumor and $CD14^+$ cells confined to establish a localized solid TiME. This tumor microenvironment (TME) model of an established tumor mass was used as it better mimics challenges seen in patients with advanced solid tumors compared with traditional tumor xenografts (18). After 12 to 14 days, when tumors measured ~100 mm^3 by caliper measurement, mice were divided into five groups ($n = 5$–6 mice/group) and injected intratumorally with three doses of 8×10^6 unmodified, $TIGIT^{KO}$, GD2.CAR-NK, and $TIGIT^{KO}$-GD2.CAR-NK or no NK cells. Each dose was injected every 5 days. Tumor growth was measured 2 to 3 times weekly by caliper measurements. IL15 was also injected intraperitoneally 2 to 3 times weekly (1 μg/mouse) to enable NK cell survival. In experiments examining the ability of $TIGIT^{KO}$GD2.CAR-NKs to persist in the TiME, tumors were harvested from mice ($n = 3$/group) 4 days after the first NK cell dose. Tumors were digested, counted using a hemocytometer, and stained for GD2, CD45, CD16, CD3, 1A7, and TIGIT. Data were acquired via flow cytometry with absolute cell counts measured by multiplying the frequencies of various cell populations by the total cell count enumerated prior to flow cytometry. The animal protocol was approved by the Baylor College of Medicine Institutional Animal Care and Use Committee, and mice were treated in strict accordance with the institutional guidelines for animal care.

Annexin V assay

Unmodified, $TIGIT^{KO}$, GD2.CAR-NK, and $TIGIT^{KO}$GD2.CAR-NK cells were co-cultured in a prepared CHLA255 TiME for 72 hours. After incubation, NK cells were stained with DNAM-1, 1A7, and TIGIT prior to being resuspended in annexin V binding buffer (BD Biosciences) and subsequent staining with annexin V (BioLegend) for 15 minutes in the dark at room temperature. Data were acquired on FACSCanto II (BD Biosciences) and analyzed using FlowJo software v11. To determine viability, NK cells were stained with 7-AAD just prior to sample acquisition on the flow cytometer.

Caspase-3/7 assay

Unmodified, $TIGIT^{KO}$, GD2.CAR-NK, and $TIGIT^{KO}$GD2.CAR-NK cells were co-cultured in a prepared CHLA255 TiME for 72 hours. After incubation, NK cells were stained with NKp46, 1A7, and TIGIT prior to being stained with caspase-3/7 (CellEvent Caspase-3/7 Green Flow Cytometry Assay Kit, Invitrogen, Cat. #C10740) for 25 minutes at 37°C followed by SYTOX AADvanced (Invitrogen, Cat. #S10349) for 5 minutes at 37°C to assess viability. Data were acquired on FACSCanto II (BD Biosciences) and analyzed using FlowJo software v11.

p-mTOR assay

Unmodified, $TIGIT^{KO}$, GD2.CAR-NK, and $TIGIT^{KO}$GD2.CAR-NK cells were co-cultured in a prepared CHLA255 TiME for 72 hours. After incubation, NK cells were stained with NKp46, 1A7, and TIGIT prior to being stained, fixed, and permeabilized followed by p-mTOR staining as detailed above. Data were acquired on FACSCanto II (BD Biosciences) and analyzed using FlowJo software v11.

Mitochondrial mass assay

Unmodified, $TIGIT^{KO}$, GD2.CAR-NK, and $TIGIT^{KO}$GD2.CAR-NK cells were co-cultured in a prepared CHLA255 TiME for 72 hours. After incubation alone or with the TiME, NK cells were stained with CD16, 1A7, and TIGIT prior to being stained with a mitochondrial labeling dye (MitoTracker Green FM Dye, Invitrogen, Cat. #M7514) for 30 minutes at 37°C. Data were acquired on FACSCanto II (BD Biosciences) and analyzed using FlowJo software.

Cell avidity assay

CHLA255 cells were seeded into a poly-L-lysine–coated (Sigma-Aldrich) piezo chip from LUMICKS. CHLA255 cells were allowed to adhere for 2 hours. Unmodified, $TIGIT^{KO}$, GD2.CAR-NK, and $TIGIT^{KO}$GD2.CAR-NK cells were labeled with CellTrace Far Red (Invitrogen, Cat. #C34564) at a 1:1,000 dilution. The CHLA255-bound piezo chip was loaded onto the z-Movi single-cell avidity analyzer. CellTrace-labeled NK cells were injected into the chip and allowed to incubate on the CHLA255 cells for 5 minutes. Afterward, NK cells were subjected to increasing acoustic force ramp from 0 to 1,000 pN over 3 minutes. Individual NK cells were observed, and the force requirement for detachment was determined based on any individual NK cell leaving the focal plane, as previously described (22).

NanoString gene expression analysis

Unmodified, $TIGIT^{KO}$, GD2.CAR-NK, and $TIGIT^{KO}$GD2.CAR-NK cells were co-cultured with CHLA255. RNA was extracted from NK cells prior to tumor exposure and after 72 hours of tumor exposure and CHLA255 depletion (EasySep PE Positive Selection Kit II, STEMCELL Technologies, Cat. #17684). RNA eluates were stored at −20°C until further processing. When ready, samples were analyzed at the Baylor College of Medicine Genomic and RNA Profiling Core on the NanoString genomics platform. Results were analyzed using nCounter Advanced Analysis software in conjunction with nSolver Analysis software (RRID: SCR_003420).

Time-lapse imaging microscopy in nanowell grids assay

Nanowell arrays on a chip were fabricated as previously reported (23). The chip was placed in a plasma chamber (Harrick Plasma Inc.) for 2 minutes and treated with PLL[20]-g[3.5]- PEG(2)/PEG(3.4)- biotin(50%) (SuSoS). Target and effector cells were washed three times with PBS prior to staining. The target (CHLA255 tumor) and effector (CAR-NK) cells were labeled with PKH26 red (Sigma-Aldrich, Cat. #PKH26GL-1KT) and PKH67 green (Sigma-Aldrich, Cat. #PKH67GL-1KT), respectively. The cells were then washed three times in full media and resuspended at a density of 1 million cells/mL. The effector and target cells were loaded onto the nanowell arrays and resuspended in Iscove's modified Dulbecco's medium, 10% FBS, and Annexin V Alexa Fluor 647. No cytokines were added. The chip was imaged with bright-field microscopy, fluorescence microscopy with Alexa Fluor 488, and Texas Red and Cy5 dyes using a Zeiss Axio Observer (Oberkochen, Germany) for 10 hours over 99 time points. Image analysis and cell tracking were performed as previously reported (24).

Statistical analysis

All numerical data are represented as mean ± SEM of either number of donors or experimental replicates, as indicated. An The unpaired two-tailed t test, paired two-tailed t test, one-way or two-way ANOVA with the Tukey multiple comparison test, log-rank (Mantel–Cox) test, and χ^2 test as indicated were used to determine the significance of differences between means, with $P < 0.05$ representing a significant difference. All statistical analyses were performed using GraphPad Prism version 10.4.2 (RRID: SCR_002798).

Data availability

The data generated in this study are available upon request from the corresponding author. Transcriptomic data on various human NK cell populations before and after exposure to TiME conditions were uploaded to Gene Expression Omnibus (RRID: SCR_005012; accession number: GSE288177).

Results

TIGIT is persistently upregulated upon NK cell activation during *ex vivo* CAR-NK manufacture

To assess the effect of NK cell activation and expansion requirements for CAR-NK manufacture on TIGIT expression, we co-cultured human peripheral blood NK cells with the K562-mb15-41BB-L feeder cell line in the presence of 500 IU/mL IL2 for 7 days and assessed TIGIT expression using flow cytometry. TIGIT was upregulated on activated/expanded NK cells in each donor examined in both the percentage of NK cells in the population that expressed TIGIT and the level of surface TIGIT per NK cell (**Fig. 1A**). TIGIT expression has historically been viewed to be activation dependent, but these data are limited to endogenous NK cells. To determine the fate of TIGIT expression on *ex vivo* activated/expanded NK cells, we examined TIGIT expression over time on activated NK cells. NK cells that received no further activation for 7 days continued to express elevated levels of TIGIT (**Fig. 1B**). NK cells that received additional activating signals via 100 IU/mL IL2 similarly expressed elevated levels of TIGIT but to no higher levels than NK cells without additional stimulation, suggesting the persistence of TIGIT expression on NK cells expanded for CAR-NK manufacture. To determine if TIGIT upregulation in NK cells was a result of our specific NK activation/expansion protocol, we assessed NK cell TIGIT expression using two other published protocols commonly used to activate and expand NK cells: K562-CD80-CD86-41BB-L feeder cells plus recombinant IL-21 (25) and the recombinant cytokine cocktail of IL12 + IL15 + IL18 known to induce memory-like NK cells for adoptive transfer (26). The NK cell expansion rate mediated by each expansion protocol was consistent with previous reports (**Fig. 1C**), reflecting adequate activation/expansion. Although not statistically significant for the other published methods, TIGIT expression was upregulated in all three expansion systems (**Fig. 1D**), suggesting that TIGIT upregulation is seen consistently during *ex vivo* activation/expansion irrespective of the type of NK manufacturing protocol used. Having characterized TIGIT upregulation on NK cells developed for therapeutic purposes, we next wanted to profile the expression of the most common TIGIT ligands, CD155 and CD112, in patients with GD2+ solid tumors. We assessed inhibitory myeloid cells and tumor cells from freshly resected pediatric neuroblastoma tissue obtained at first resection for CD155 and CD112 expression. MDSCs and M2-TAMs were found to highly express both CD155 and CD112, reproducibly at levels higher than tumor cells themselves (**Fig. 1E**). Our combined data suggest that the TIGIT–TIGIT ligand axis has the potential to inhibit the function of adoptively transferred therapeutic NK cells in solid tumors.

Genetic deletion of TIGIT does not alter CAR-NK expansion or phenotype

Given persistent elevation in TIGIT in NK cells undergoing activation/expansion protocols for CAR-NK manufacture and the high expression of TIGIT ligands in solid TiMEs, we hypothesized that deletion of TIGIT would improve CAR-NK efficacy by rendering CAR-NKs resistant to inhibitory signaling. We developed a sequential CRISPR/Cas9 and retroviral transduction protocol to delete TIGIT in human CAR-NKs. Primary human peripheral blood NK cells were expanded with a K562-mb15-41BB-L feeder cell line and IL2 for 6 days. Using electroporation, we delivered a payload of Cas9 protein and two gRNAs targeting exon 2 of *TIGIT* in expanded NK cells. This was followed immediately by retroviral transduction of NK cells with a published GD2-targeting CAR (**Fig. 2A**; ref. 13). Using this approach, we consistently achieved >90% TIGIT knockout efficiency (on average 84% TIGIT+ cells in GD2.CAR-NK vs. 6.5% TIGIT+ cells in TIGIT^{KO}GD2.CAR-NK) and >60% GD2.CAR transduction efficiency (on average 60.8% in GD2.CAR-NKs vs. 63.4% TIGIT^{KO}GD2.CAR-NKs; **Fig. 2B and C**; Supplementary Fig. S1B and S1C). To determine if TIGIT deletion affected proliferation during manufacture, we expanded TIGIT^{KO}CAR-NKs with K562-mb15-41BB-L and IL-2. No significant differences were seen in fold expansion of TIGIT^{KO}GD2.CAR-NKs compared with GD2.CAR-NKs (on average 83-fold expansion for TIGIT^{KO}-GD2.CAR-NK versus 73-fold expansion for GD2.CAR-NK) after 7 days of expansion with the K562-mb15-41BB-L feeder cell line in the presence of 100 IU/mL (**Fig. 2D**). NK cells express multiple activating and inhibitory germline-encoded receptors that hold key functions in enabling NK cell cytotoxicity. We assessed if TIGIT deletion in generated GD2.CAR-NKs altered their expression of activating and inhibitory receptor repertoires. TIGIT deletion did not alter the surface expression of the activating receptors DNAM-1 and NKG2D and the inhibitory receptors NKG2A, TIM-3, PD-1, or LAG-3 on TIGIT^{KO}GD2.CAR-NKs after *ex vivo* manufacture (**Fig. 2E**).

TIGIT deletion in GD2.CAR-NKs improves antitumor activity

To evaluate their antitumor activity, TIGIT^{KO}GD2.CAR-NKs were co-cultured with GFP-expressing CHLA255 neuroblastoma for 96 hours in an NK cell–favoring ratio [effector-to-target (E:T) of 4:1] and a tumor-favoring ratio (E:T of 1:4). Whereas all NK cell conditions successfully eliminated tumor within 24 hours at NK cell–favoring ratios, only TIGIT^{KO}GD2.CAR-NKs eliminated tumor at tumor-favoring ratios and exhibited superior tumor-killing kinetics, regressing tumor within 12 hours compared with no tumor regression by GD2.CAR-NKs (**Fig. 3A**). To assess if upregulation of activating receptors, downregulation of inhibitory receptors, or changes in CAR expression contributed to the enhanced tumor killing by TIGIT^{KO}GD2.CAR-NKs, we assessed NK cell receptor expression before and after tumor co-culture. After 96 hours of tumor exposure, no differences were observed in GD2 CAR expression between TIGIT-expressing CAR-NKs and TIGIT^{KO}-GD2.CAR-NKs (**Fig. 3B**). Additionally, no significant changes were observed in the expression of DNAM-1, NKG2D, NKG2A, TIM-3, PD-1, or LAG-3 on TIGIT^{KO}GD2.CAR-NKs after tumor exposure when compared with their expression on GD2.CAR-NKs (**Fig. 3C**). TIGIT deletion did not result in increased degranulation (CD107a), IFN-γ expression, or Fas-L expression on GD2.CAR-NK after long-term culture (**Fig. 3D–F**). Overall, TIGIT deletion did not result in any significant compensatory changes in NK receptors or receptor functions that would account for the observed enhanced CAR-NK tumor control.

TIGIT^{KO}GD2.CAR-NKs limited tumor growth and expanded in the presence of immunosuppressive myeloid cells

To evaluate the effect of TIGIT deletion on the antitumor activity of CAR-NKs in a microenvironment that mimics TiME

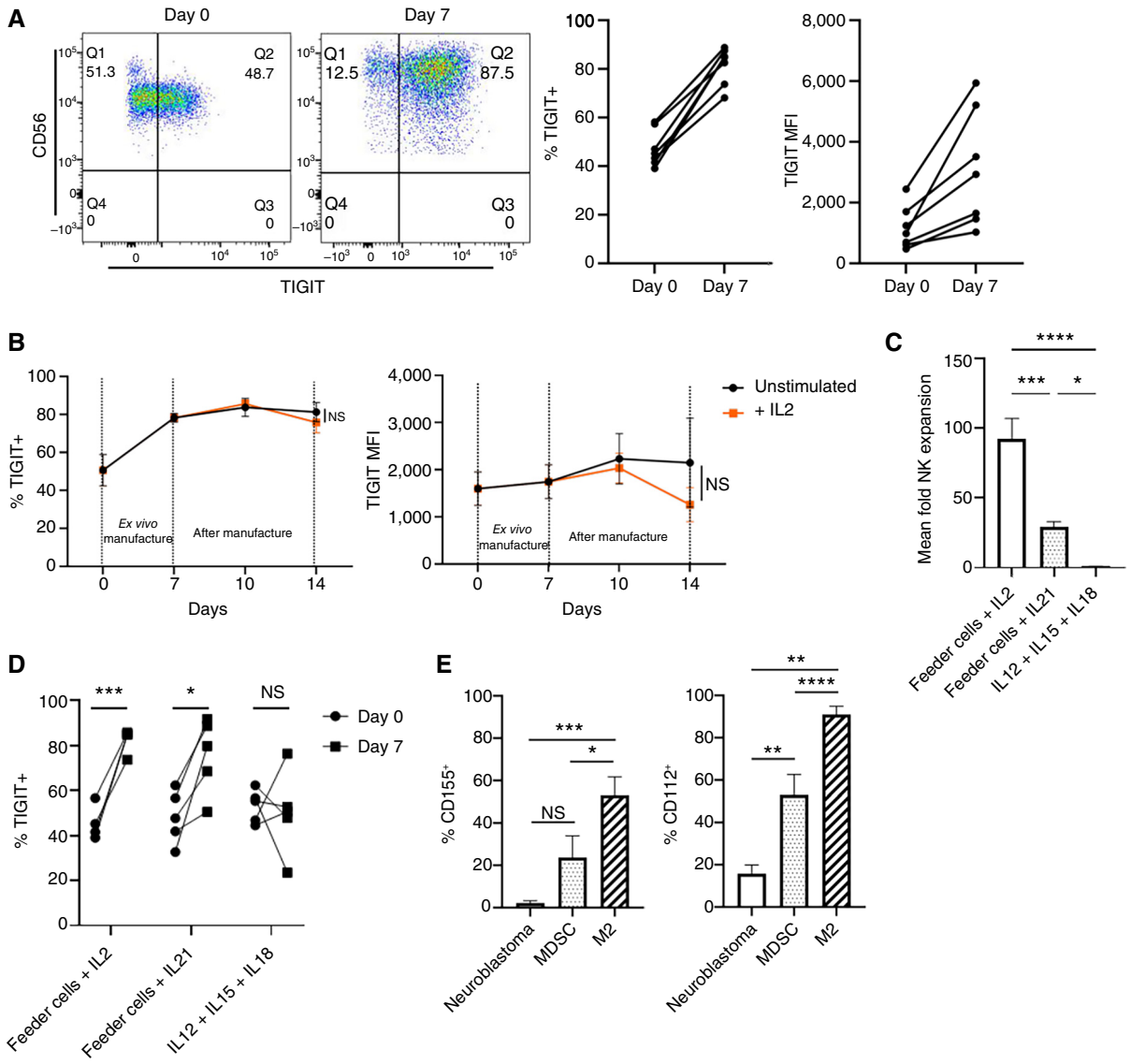

Figure 1.

TIGIT is upregulated in human NK cells undergoing activation and expansion for CAR-NK manufacture. **A,** Representative flow cytometric dot plot from a single donor (left) and mean change in TIGIT expression on PBMC-derived $CD56^{+}CD3^{-}$ NK cells from $n = 7$ healthy donors before (day 0) and after 7 days (day 7) of activation/expansion using the feeder cell line K562-mb15-41BB-L and IL2. **B,** Change in TIGIT expression on NK cells over time during and after *ex vivo* manufacture with and without IL2 ($n = 5$ healthy blood donors). **C,** Mean fold expansion of NK cells after 7 days of activation using K562-mb15-41BB-L and IL2, K562-41BB-L and IL21, or IL12 + IL15 + IL18 cytokine cocktail ($n = 4$–5 healthy donors). **D,** Flow cytometric analysis of TIGIT expression before and after 7 days of activation using K562-mb15-41BB-L and IL2, K562-41BB-L and IL21, or IL12 + IL15 + IL18 cytokine cocktail ($n = 4$–5 healthy donors). **E,** Mean TIGIT ligand CD155 and CD112 expression from $n = 6$ patients on tumor cells (neuroblastoma), MDSCs, and M2 macrophages (M2) from freshly resected pediatric neuroblastoma tissue. *, $P < 0.05$; **, $P < 0.01$; ***, $P < 0.001$; ****, $P < 0.0001$; NS, nonsignificant. MFI, mean fluorescence intensity.

immunosuppression and the increased TIGIT ligand expression seen in patient tumors, we co-cultured CAR-NKs with the TIGIT ligand–expressing NK cell–insensitive neuroblastoma line, LA-N-1, in combination with TIGIT ligand–expressing monocyte-derived MDSCs for 24 hours at an effector:tumor:myeloid ratio of 1:2:2 (Supplementary Fig. S2A–S2C). The inclusion of MDSCs in tumor co-cultures led to decreased CD107a and IFNγ expression by GD2.CAR-NKs. In contrast, $TIGIT^{KO}$GD2.CAR-NKs maintained IFNγ expression. However, TIGIT deletion did not reverse inhibition of GD2.CAR-NK degranulation. In the presence of tumor and MDSCs, GD2.CAR-NKs exhibited decreased CD107a degranulation, and IFNγ production as compared with that in the presence of tumor alone, reflecting MDSC-based immunosuppression (**Fig. 4A**). In contrast, $TIGIT^{KO}$GD2.CAR-NKs maintained their ability to secrete IFNγ in the presence of tumor and MDSCs. However, no differences were observed in the percentage of NK cells

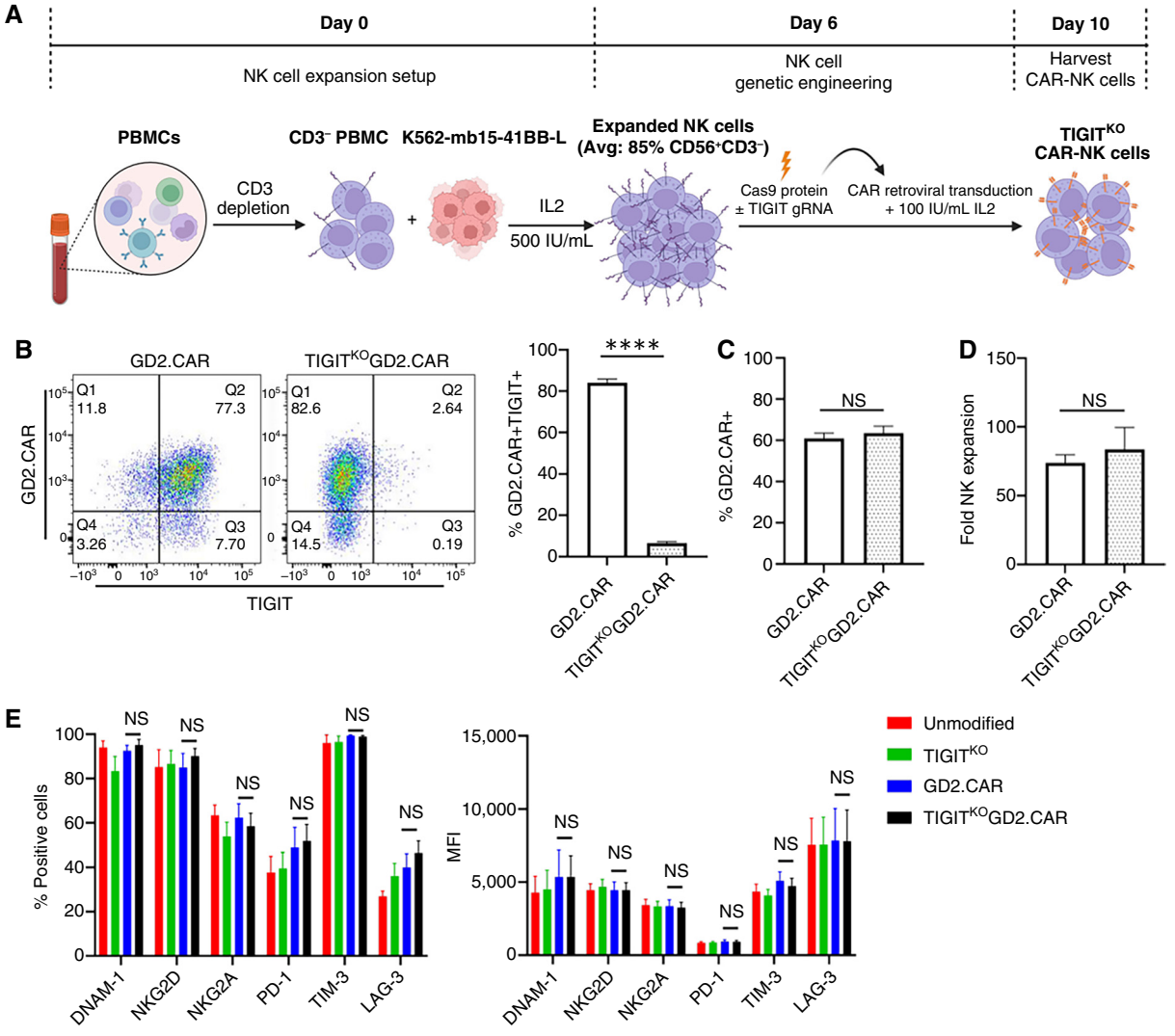

Figure 2.

Genetic engineering to generate TIGIT^{KO} CAR-NKs. **A,** Protocol used for genetic modification of human expanded CD56^{+}CD3^{-} NK cells using sequential CRISPR/Cas9 and retroviral transduction to generate TIGIT^{KO}GD2.CAR-NKs. **B,** Representative flow plots assessing CAR and TIGIT expression on GD2.CAR-NKs and TIGIT^{KO}GD2.CAR-NKs and mean TIGIT expression on GD2.CAR-NKs after manufacture from $n = 17$ healthy donors. **C,** Mean GD2.CAR expression on TIGIT-expressing and TIGIT^{KO} NK cells from $n = 17$ healthy donors. **D,** Mean fold expansion of GD2.CAR-NKs and TIGIT^{KO}GD2.CAR-NKs after 7 days of activation using K562-mb15-41BB-L and IL2 from $n = 3$ healthy donors. **E,** Mean DNAM-1, NKG2D, NKG2A, PD-1, TIM-3, and LAG-3 expression on unmodified NK cells, TIGIT^{KO} NK cells, GD2.CAR-NKs, and TIGIT^{KO}GD2.CAR-NKs after manufacture from $n = 6$ healthy donors. ****, $P < 0.0001$; NS, nonsignificant. MFI, mean fluorescence intensity. [**A,** Created in BioRender. Navin, I. (2024) https://BioRender.com/q68p863]

degranulating in the presence of tumor and MDSCs between TIGIT-expressing and TIGIT-deleted CAR-NKs. To more directly assess whether TIGIT deletion would enhance CAR-NK function in harsh TMEs, we developed a TiME co-culture assay that mimicked the immunosuppressive environment of solid tumors with suppressive myeloid infiltrates (Supplementary Fig. S3A). We co-cultured CD14^{+} monocytes for 3 days with a CHLA255 neuroblastoma cell line previously demonstrated to secrete high amounts of TGFβ1 and IL6, both of which have been implicated in tumor-induced polarization of intratumor myeloid cells (27–29). After 3 days of co-culture, the monocytes were skewed to an inhibitory M2-TAM–like phenotype (Supplementary Fig. S3B–S3D). The inclusion of tumor-influenced M2-TAMs produced a highly immunosuppressive environment that resulted in decreased CAR-NK tumor cytotoxicity compared with that of CAR-NKs in tumor cultures without M2-TAMs (Supplementary Fig. S3E and S3F). To this established TiME co-culture, we added TIGIT^{KO}-GD2.CAR-NKs (manufactured from the same donor as the macrophages in the TiME co-culture to avoid alloreaction) at a tumor-favoring E:T ratio of 1:10. Unmodified NK, GD2.CAR-NK, and TIGIT^{KO} NK cells without a CAR were used as controls. TIGIT^{KO}GD2.CAR-NKs displayed robust tumor killing, enhanced killing kinetics, and both early and rapid expansion compared with controls in this TiME culture system (**Fig. 4B** and **C**). To improve the rigor of the study, the enhanced anti-tumor kinetics conferred by TIGIT deletion in the TiME was

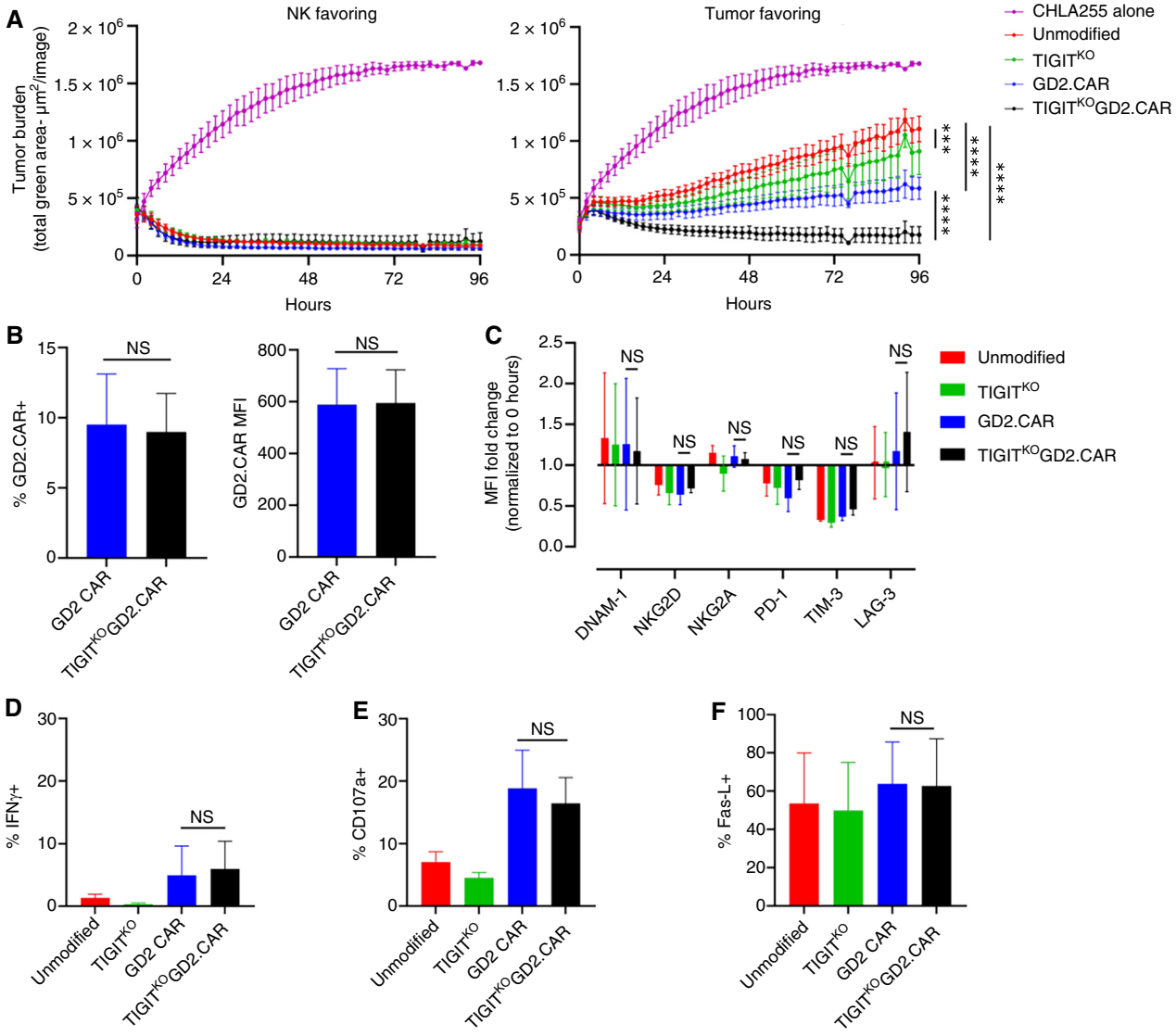

Figure 3.

TIGIT^{KO}GD2.CAR-NKs exhibit enhanced tumor control *in vitro*. **A,** GFP-expressing CHLA255 neuroblastoma cells were co-cultured with TIGIT^{KO}GD2.CAR-NKs for 96 hours at an E:T ratio of 4:1 (NK favoring) or 1:4 (tumor favoring). Mean (from $n = 4$ healthy donors) tumor growth when cultured without effector (purple) or with unmodified NK cells (red), TIGIT^{KO} NK cells (green), GD2.CAR-NKs (blue), or TIGIT^{KO}GD2.CAR-NKs (black) was analyzed using Incucyte AUC followed by one-way ANOVA with the Tukey multiple comparisons test. **B,** Mean GD2.CAR expression on TIGIT-expressing and TIGIT^{KO} NK cells after tumor co-culture from $n = 3$ healthy donors. **C,** Mean fold change in DNAM-1, NKG2D, NKG2A, TIM-3, PD-1, or LAG-3 expression on unmodified, TIGIT^{KO}, GD2.CAR, and TIGIT^{KO}GD2.CAR-NKs after tumor co-culture ($n = 3$ healthy blood donors). **D,** Mean IFNγ expression in unmodified, TIGIT^{KO}, GD2.CAR, and TIGIT^{KO}GD2.CAR-NKs after tumor co-culture from $n = 3$ healthy donors. **E,** Mean CD107a expression on unmodified, TIGIT^{KO}, GD2.CAR, and TIGIT^{KO}GD2.CAR-NKs after tumor co-culture from $n = 3$ healthy donors. **F,** Mean Fas-L expression on unmodified, TIGIT^{KO}, GD2.CAR, and TIGIT^{KO}GD2.CAR-NKs after tumor co-culture from $n = 3$ healthy donors. ***, $P < 0.001$; ****, $P < 0.0001$; NS nonsignificant. MFI, mean fluorescence intensity.

also validated in HER2.CAR-NKs against the HER2+ lung cancer cell line H1650 (Supplementary Fig. S4A). As in previous assays, these enhancements were not due to increased expression of the CAR or changes in expression of NK cell germline receptors (**Fig. 4D** and **E**). We next evaluated the ability of TIGIT^{KO}GD2.CAR-NKs to control tumor after repeated TiME exposure, assessing their ability to mediate effective serial killing. TIGIT^{KO}GD2.CAR-NKs were co-cultured over three sequential 72-hour TiME co-cultures. Consistent with our previous data, TIGIT^{KO}GD2.CAR-NKs exhibited improved tumor killing in the first TiME co-culture compared with GD2.CAR-NKs (**Fig. 4F**, TiME #1). Although all control conditions failed to control tumor in successive TiME co-cultures, TIGIT^{KO}GD2.CAR-NKs exhibited the best tumor control (**Fig. 4F**, TiME #2) but eventually faltered with successive challenge (**Fig. 4F**, TiME #3).

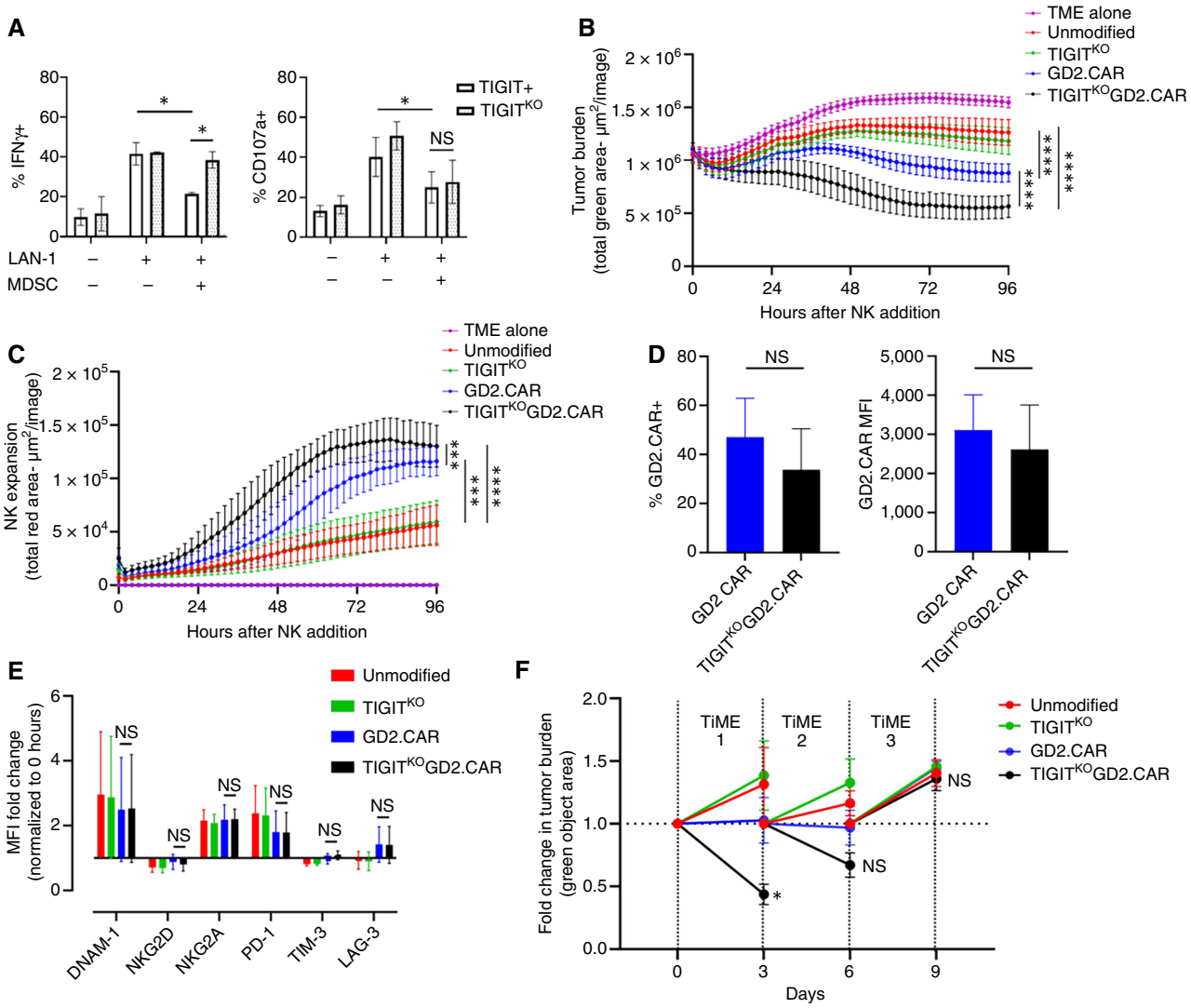

Figure 4.

TIGIT^{KO}GD2.CAR-NKs expand and eliminate neuroblastoma in a TIGIT ligand–rich environment. **A,** Mean IFNγ and CD107a expression in GD2.CAR-NKs or TIGIT^{KO}GD2.CAR-NKs cultured with LAN-1 neuroblastoma alone or in combination with MDSCs from $n = 3$ healthy donors. **B,** GFP-expressing CHLA255 neuroblastoma cells were cultured with CD14^{+} monocytes for 72 hours (TiME establishment) prior to the addition of CellTracker Red–labeled NK cells and then further co-cultured for 96 hours. **C,** Mean tumor growth and NK cell expansion kinetics from $n = 3$–4 healthy donors in co-cultures without effector (purple) or with unmodified NK cells (red), TIGIT^{KO} NK cells (green), GD2.CAR-NK (blue), or TIGIT^{KO}GD2.CAR-NK (black) were analyzed using Incucyte. **D,** Mean GD2.CAR expression on TIGIT-expressing and TIGIT^{KO} NK cells after TiME culture from $n = 4$ healthy donors. **E,** Mean change in DNAM-1, NKG2D, NKG2A, TIM-3, PD-1, or LAG-3 expression on unmodified, TIGIT^{KO}, GD2.CAR, and TIGIT^{KO}GD2.CAR-NKs after TiME culture from $n = 3$ healthy donors. **F,** Mean fold change in neuroblastoma tumor in each of three sequential TiME rechallenge assays in which unmodified NK cells (red), TIGIT^{KO} NK cells (green), GD2.CAR-NKs (blue), and TIGIT^{KO}GD2.CAR-NKs (black) from $n = 3$ healthy donors were repetitively challenged against established TiMEs. *, $P < 0.05$; ***, $P < 0.01$; ****, $P < 0.0001$; NS, nonsignificant. MFI, mean fluorescence intensity.

TIGIT^{KO}GD2.CAR-NKs control tumor and prolong survival in mice bearing TiME xenografts

We injected NSG-SGM3 mice subcutaneously with LA-N-1 tumor admixed with CD14^{+} monocytes in Matrigel extracellular matrix solution. When tumors reached ~100 mm^3, tumors formed a suppressive TiME-like matrix rich in suppressive stroma, inhibitory myeloid cells, and a rich suppressive cytokine milieu (21). To assess the antitumor activity of TIGIT^{KO}GD2.CAR-NKs directly within a solid TiME without the confounding effects of immune cell trafficking, mice were treated with three intratumor injections of NK cells every 5 days (see **Fig. 5A** for treatment schema). Although immunosuppressive TiME xenograft–bearing mice treated with control NK cells exhibited tumor growth and early death, TIGIT^{KO}GD2.CAR-NK–treated mice experienced modest control of their tumor burden, with two of five mice experiencing durable tumor control (**Fig. 5B**) and extended survival (**Fig. 5C**). To determine if differences in GD2.CAR expression or NK persistence could explain the observed differences in response between the groups of treated mice,

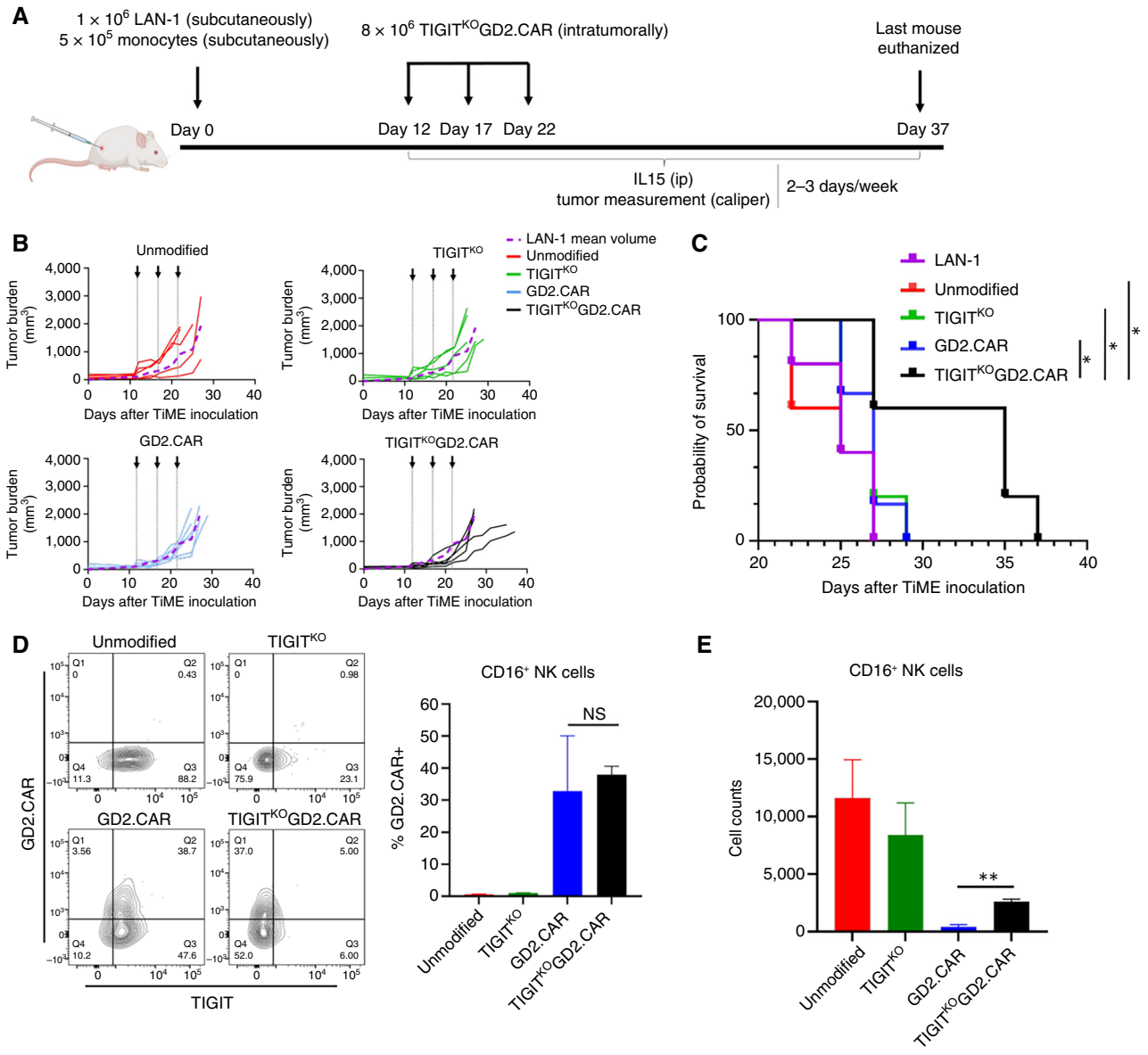

Figure 5.

TIGIT^{KO}GD2.CAR-NKs extend survival in an *in vivo* TiME xenograft mouse model. **A,** Schema for neuroblastoma TiME xenograft mouse model in NSG-SGM3 mice. Mice were inoculated subcutaneously with a 2:1 mixture of LAN-1 neuroblastoma cells and CD14^{+} monocytes. After 12 days of tumor growth (tumors ~100 mm^3), mice were injected intratumorally with TIGIT^{KO}GD2.CAR-NKs ×3 5 days apart, along with intraperitoneal (ip) injections of 1 mg of IL15 three times per week. **B,** Spider plots of tumor burden in mice treated with unmodified (red), TIGIT^{KO} (green), GD2.CAR-NK (blue), or TIGIT^{KO}GD2.CAR-NK (black) compared with mean tumor burden of untreated mice (purple; $n = 6$ mice/group). **C,** Survival curves of mice treated with unmodified (red), TIGIT^{KO} (green), GD2.CAR-NK (blue), or TIGIT^{KO}GD2.CAR-NK (black). **D,** Representative flow cytometric contour plots (left) and mean GD2.CAR expression on TIGIT-expressing and TIGIT^{KO} NK cells within tumor digests harvested on day 16 ($n = 3$ mice/group). **E,** Mean number of absolute intratumoral NK cells quantified from tumor digests ($n = 3$ mice/group). *, $P < 0.05$; **, $P < 0.01$; NS, nonsignificant.

tumors were harvested 4 days after the first NK cell injection and analyzed using flow cytometry. Although we observed no differences in GD2 CAR expression on intratumor NK cells among the CAR-containing groups (32.8% on GD2.CAR-NKs and 37.9% on TIGIT^{KO}-GD2.CAR-NKs; **Fig. 5D**), there were higher numbers of intratumor CAR-NKs in mice treated with TIGIT^{KO}GD2.CAR-NKs compared with those treated with GD2.CAR-NKs (**Fig. 5E**).

TIGIT^{KO}GD2.CAR-NKs downregulate genes associated with cell adhesion and exhibit decreased CAR-mediated synapses with tumor

TIGIT deletion in CAR-NKs enhances CAR-NK expansion and ability to control tumor in harsh TiMEs despite similar levels of degranulation, CAR molecule expression, and Fas-L surface expression. We also observed comparable levels of caspase-3/7,

annexin V, mitochondrial mass, and p-mTOR (Supplementary Fig. S4B–S4E). Furthermore, the contribution of the receptor DNAM-1, an activating receptor that competes with TIGIT for its ligands, was inconsequential to CAR-NK antitumor activity upon TIGIT deletion in NK cells (Supplementary Fig. S4F). To determine how TIGIT improved CAR-NK activity in the TME, we performed bulk global gene expression analysis. We isolated total RNA from unmodified, TIGIT^{KO}, GD2.CAR-NK, or TIGIT^{KO}GD2.CAR-NK cells before and after 72 hours of co-culture with neuroblastoma tumor cells. Principal component analysis revealed that although tumor exposure affected gene expression, TIGIT deletion did not significantly alter gene expression patterns in either non-CAR or GD2.CAR-expressing NK cells (**Fig. 6A**). When comparing gene expression between TIGIT^{KO}GD2.CAR-NKs and GD2.CAR-NKs after tumor exposure, significant differences were noted in both upregulated and downregulated genes. Global gene score analysis showed decreased expression of genes related to cell adhesion, apoptosis, and oxidative stress response in TIGIT^{KO}GD2.CAR-NKs (**Fig. 6B**). Consistent with the robust downregulation in cell adhesion score, the gene encoding the cell adhesion and immunologic synapse protein VCAM-1 was the most downregulated gene in TIGIT^{KO}GD2.CAR-NKs (**Fig. 6C**; Supplementary Fig. S4G and S4H). To verify that this downregulation resulted in reduced percentage of VCAM-1 surface protein expression, we co-cultured TIGIT^{KO}GD2.CAR-NKs or control NKs with CHLA255 for 72 hours. We observed no significant downregulation of VCAM-1 protein in non–CAR-expressing NKs, irrespective of TIGIT expression. In contrast, compared with TIGIT-expressing GD2.CAR-NKs, TIGIT^{KO}-GD2.CAR-NKs exhibited lower levels of surface VCAM-1 protein (**Fig. 6D**; Supplementary Fig. S4I). An assessment of its expression level per NK cell revealed a modest decrease in surface VCAM-1 on both non-CAR and CAR-NK cells after CHLA255 exposure for 72 hours.

Given these data suggesting differences in NK adhesion to targets, we wanted to directly test the effect of TIGIT deletion on immune synapse strength. We first evaluated NK cell structural avidity at the single-cell level using a LUMICKS z-Movi cell avidity analyzer, which measures the binding force between effector and target cells, to determine if TIGIT deletion alters CAR-NK interactions with tumors via synapse formation or release. NK cells lacking TIGIT (either non-CAR or CAR-expressing) exhibited lowered binding capacities to CHLA255 compared with their TIGIT-expressing counterparts (**Fig. 7A**). We further interrogated the effect of TIGIT deletion on synapse stability by using the time-lapse imaging microscopy in nanowell grids assay (23, 24). We utilized this assay to evaluate the duration of GD2.CAR-NK cell–mediated synapses against CHLA255 neuroblastoma and the resulting time taken to mediate tumor death (**Fig. 7B**). We assessed the time of contact between NK cells and tumor targets ($T_{Contact}$) and the time taken by NK cells to induce tumor cell death (T_{Death}) in nanowells at an E:T ratio of 1:1 (**Fig. 7C**). When comparing NK cells without CARs, individual TIGIT^{KO} NK cells (green) exhibited reduced duration of contact with the tumor cells (138 ± 12 minutes, mean ± SEM) in comparison with unmodified NK cells (198 ± 12 minutes; **Fig. 7C**). Similarly, individual TIGIT^{KO} NK cells also killed tumor cells faster (120 ± 18 minutes) in comparison with unmodified NK cells (192 ± 24 minutes; **Fig. 7C**). We next compared GD2.CAR-expressing NK cells using the time-lapse imaging microscopy in nanowell grids assays. Consistent with our results with non–CAR-NK cells, TIGIT^{KO}GD2.CAR-NK cells exhibited the shorter contact durations (138 ± 18 minutes, mean ± SEM) and faster killing of tumor targets (102 ± 18 minutes) compared with control GD2.CAR-NK cells, which exhibited a longer contact time (228 ± 24 minutes) with a slower kill time (138 ± 18 minutes; **Fig. 7C**).

To determine if decreased contact duration may allow for more rapid engagement of multiple tumor targets, TIGIT^{KO}GD.CAR-NKs were cultured in nanowells at E:T ratios of 1:2. In contrast to control GD2.CAR-NKs, TIGIT^{KO}GD2.CAR-NKs consistently formed successive shorter-lived functional immunological synapses with CHLA255 tumor targets (**Fig. 7D** and **E**). Consistent reductions in synapse duration between TIGIT^{KO}GD2.CAR-NKs and tumor targets were only observed in contact 1 whereas contact two exhibited a more diverse pattern of synapse durations. GD2.CAR-NK cells exhibited a longer cumulative time spent to contact and disengage from both tumor targets compared with TIGIT^{KO}GD2.CAR-NK cells (240 ± 42 minutes for GD2.CAR-NK vs. 96 ± 36 minutes for TIGIT^{KO}GD2.CAR-NK). The swift termination of the TIGIT^{KO}GD2.CAR-NK immunologic synapse did not come at the expense of its tumor cytotoxicity. Instead, we observed that a greater proportion of TIGIT^{KO}GD2.CAR-NK cells eliminated two tumor targets when compared with their TIGIT-expressing controls (87% TIGIT^{KO}GD2.CAR-NK vs. 71% GD2.CAR-NK; **Fig. 7F**). Collectively, these results from single-cell assays demonstrate that knocking out TIGIT in NK cells (with or without CAR) enables the formation of efficient synapses with tumor cells resulting in fast killing and serial killing.

Discussion

In this report, we show that human CAR-NKs from which *TIGIT* was genetically deleted evade TIGIT-mediated suppression found in solid tumor microenvironments. We demonstrate that TIGIT^{KO}-GD2.CAR-NKs exhibit both enhanced tumor control and proliferation in solid TiMEs that typically inhibit TIGIT-expressing CAR-NKs both *in vitro* and in xenograft-bearing mice. Furthermore, we present data that reveal a previously unknown role for TIGIT in modulating cell adhesion of CAR-NKs to their tumor targets. GD2.CAR-NKs without TIGIT downregulated genes associated with cell adhesion and exhibited reduced cell avidity against tumor targets, conferring a more efficient serial killing capacity to CAR-NKs. Thus, our genetic engineering approach to interrogate TIGIT-mediated effects on CAR-NKs within solid TiMEs revealed a noncanonical mechanism by which TIGIT affects NK cells expressing CARs and enabled an approach that might improve the efficacy of CAR-NKs targeting solid tumors.

Our study reveals different mechanisms than canonical TIGIT signaling by which TIGIT may impair CAR-mediated function in NK cells. Previous studies have used antibody blockade of CD155, CD112, or TIGIT in murine and human endogenous NK cells (30, 31). These studies suggested that TIGIT inhibited NK cell antitumor activity by acting as a competitive receptor to the activating receptor DNAM-1, which also binds CD155 or CD112 on tumors, and thereby blocking DNAM-1–based activation of NK cells (32, 33). In contrast to endogenous NK cells, our data suggest that DNAM-1 activation is not involved in enhancing NK cytotoxicity in the context of CAR-NKs, in which the additional activating signals through the CAR molecule likely override any benefit from DNAM-1. Canonical TIGIT signaling also inhibits AKT-dependent survival via reduced apoptosis (34), activates the mTOR pathway, and upregulates genes associated with glycolysis (35). However, loss of TIGIT signaling in CAR-NKs did not increase phosphorylated mTOR nor result in apoptotic resistance or increased mitochondrial

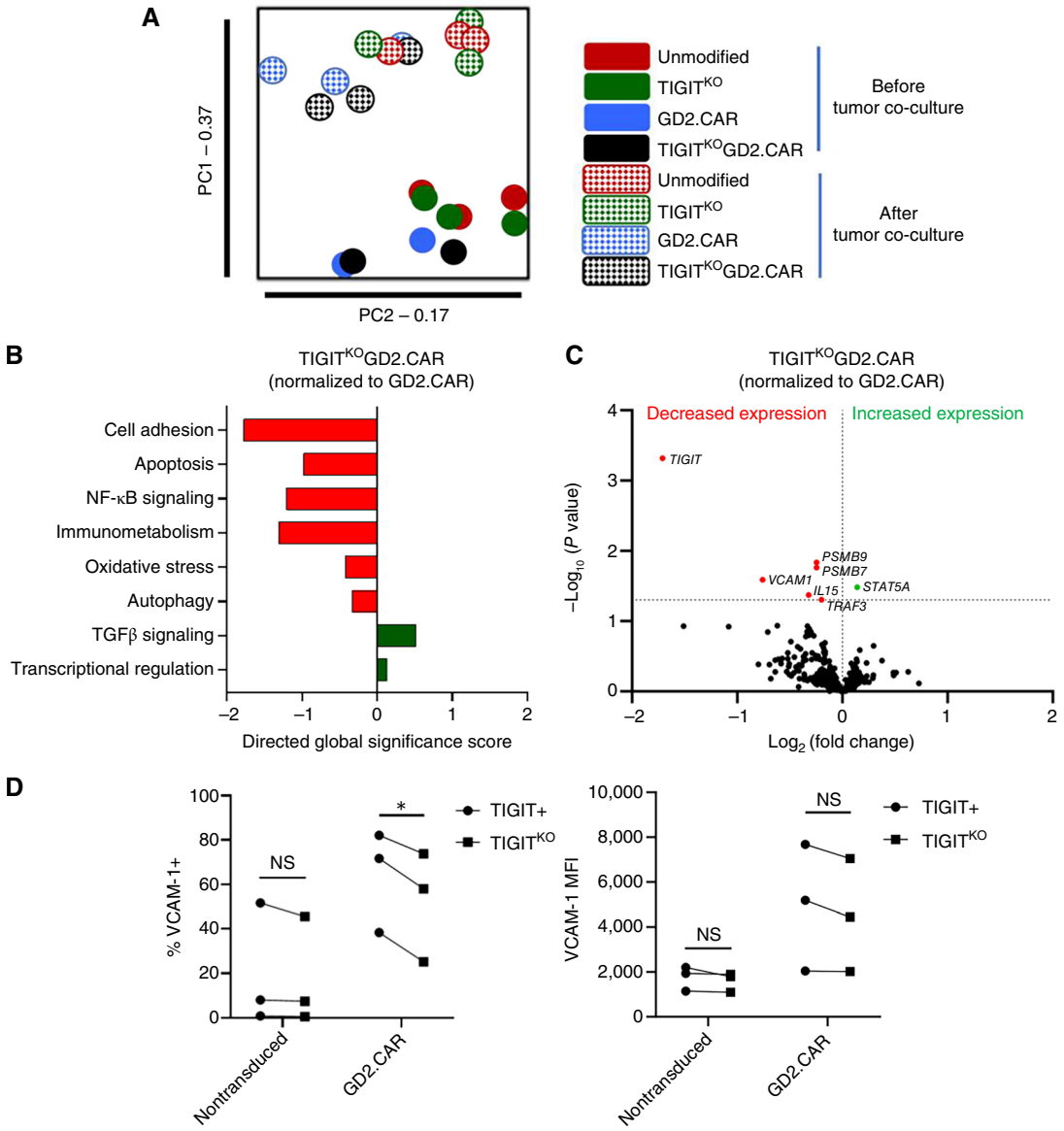

Figure 6.

Transcriptome and cell adhesion analysis of TIGIT^{KO}GD2.CAR-NKs after tumor co-culture. **A,** RNA isolation of NK cells was performed before and after 72-hour tumor co-culture and transcriptomic changes quantified using NanoString. Principal component analysis of gene expression in unmodified, TIGIT^{KO}, GD2.CAR-NK, and TIGIT^{KO}GD2.CAR-NKs before and after co-culture. **B,** Gene Ontology of TIGIT^{KO}GD2.CAR-NK gene expression compared with control GD2.CAR-NKs after tumor exposure ($n = 3$ healthy blood donors). **C,** Volcano plot analysis of TIGIT^{KO}GD2.CAR-NK gene expression compared with control GD2.CAR-NK cells after tumor exposure ($n = 3$ healthy blood donors). **D,** Percentage of VCAM-1 and mean fluorescence expression on unmodified, TIGIT^{KO}, GD2.CAR-NK, and TIGIT^{KO}GD2.CAR-NKs after 72-hour CHLA255 tumor co-culture ($n = 3$ healthy blood donors). *, $P < 0.05$; NS, nonsignificant. MFI, mean fluorescence intensity.

mass typically regulated by AKT (36). Taken together, our data suggest that the canonical inhibitory TIGIT signaling typically responsible for the impairment of NK cytotoxicity is not responsible for CAR-NK inhibition and that an alternate role for TIGIT may exist specifically in the context of CAR expression.

Indeed, our data suggest that TIGIT may modulate CAR-NK adhesion to tumor targets. Previous work has shown that when endogenous NK cells engage targets via their natural receptors, TIGIT rapidly localizes to synapses rich in TIGIT ligands on target cells, thus preventing DNAM-1 from binding TIGIT ligands and activating NK cytotoxicity (37, 38). In NK cells modified to express CARs, our data suggest that TIGIT localization to CAR-containing synapses does not serve to outcompete DNAM-1 but to enhance cell adhesion and cell avidity to tumor targets. Hence, the improved tumor control resulting from TIGIT deletion on CAR-NKs is not dependent on DNAM-1 activation and enhanced cytotoxic potential but rather on diminished VCAM-1–mediated cell adhesion and weakened cell avidity, which potentially allows for improved serial

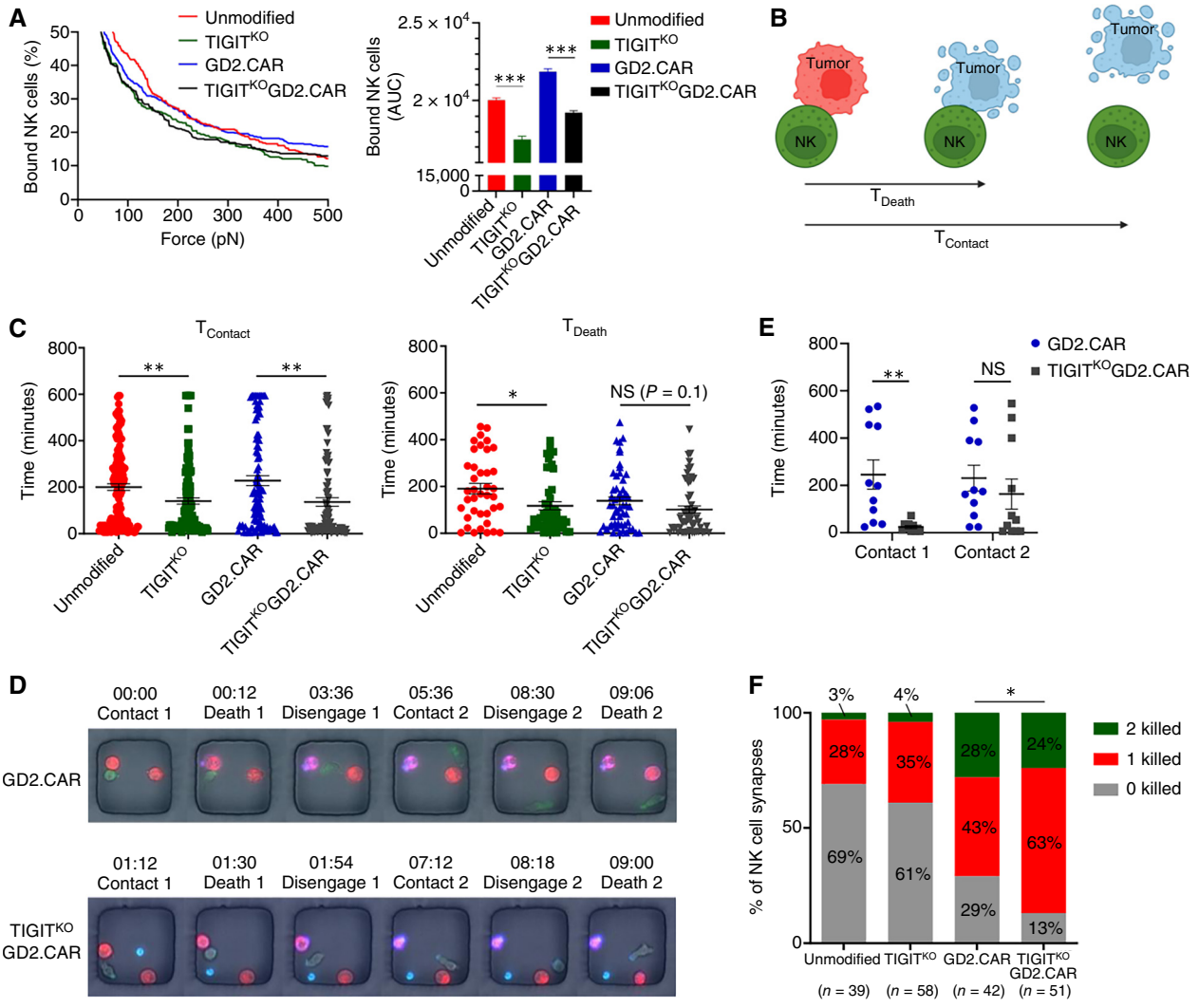

Figure 7.

TIGIT deletion reduces GD2.CAR-NK cell synapse duration with tumor targets. **A,** Mean number of bound NK cells to CHLA255 tumor targets to measure cell avidity of unmodified, TIGIT^{KO}, GD2.CAR-NK, and TIGIT^{KO}GD2.CAR-NKs to target cells ($n = 3$ replicates). **B,** Schematic representation for the time-lapse imaging microscopy in nanowell grids assay. Unmodified, TIGIT^{KO}, GD2.CAR-NK, and TIGIT^{KO}GD2.CAR-NKs (PKH26 green cell membrane label); CHLA255 tumor cells (PKH67 red cell membrane label) at 1E:1T and 1E:2T ratios. Annexin V (blue) marker for tumor cell death. **C,** Duration of synapse ($T_{Contact}$) and time to tumor death (T_{Death}) of all encounters in nanowells containing a 1E:1T ratio (n = 91–143 single cells). **D,** Representative micrographs of GD2.CAR-NK (top) and TIGIT^{KO}GD2.CAR-NK (bottom) interacting with CHLA255 tumor cells. **E,** Duration of individual synapse times of GD2.CAR-NK and TIGIT^{KO}GD2.CAR-NKs with CHLA255 from nanowells with 1E:2T ratios (n = 10–11). **F,** Proportion of unmodified, TIGIT^{KO}, GD2.CAR-NK, and TIGIT^{KO}GD2.CAR-NKs that killed 0, 1, or 2 tumor targets from nanowells with a 1E:2T ratio (n = 39–58 replicates). *, $P < 0.05$; **, $P < 0.01$; ***, $P < 0.001$; NS, nonsignificant. [**B,** Created in BioRender. Navin, I. (2025) https://BioRender.com/r39c558]

killing and more efficient tumor destruction. Mechanistically, the weakening of VCAM-1–based adhesion and avidity by loss of TIGIT at the immune synapse may occur because of decreased TIGIT-mediated inhibition of regulators of PI3K activity resulting in downregulation of LFA-1, a critical initiator of NK cell synapse formation (39, 40). However, it is unlikely that the impact of TIGIT deletion is solely limited to the regulation of adhesion molecules. The mere absence of TIGIT, a high-affinity, synapse-localized receptor, may directly affect the avidity of CAR-NK cells with tumor targets by rendering inability to engage with CD155 and CD112 on the tumor. Our data showed that this weakened avidity was partially rescued after contact with subsequent tumor targets. This suggests that mechanisms directing the accelerated kinetics of the first CAR-NK–tumor synapses may be different from those that regulate subsequent synapses. This altered avidity might be influenced by the dynamic changes in the levels of intracellular ATP and serine/threonine kinases, as well as extracellular shuttling dynamics of CAR molecules which are critical to the maintenance of the immunologic synapse (18, 41). Additionally, under excess ligand availability, increased synaptic localization of DNAM-1 may engage more efficiently to slightly enhance CAR-NK adhesion over multiple rounds of serial tumor killing. This highlights the utility of an

alternate mechanism to enhance CAR-NK activity relative to previous approaches that attempted to improve CAR-NK cytotoxicity by strengthening immune synapse formation (22). Although increased cell avidity has typically been perceived as beneficial to CAR-mediated tumor killing, recent studies have shown that CAR-T cells possessing intermediate binding avidity compared with those with high avidity for their targets displayed the best tumor control owing to increased serial killing activity (42–45). Thus, the reduction in synapse strength exhibited by TIGIT^{KO}GD2.CAR-NKs allowing faster detachment times and more rapid serial killing may allow improved overall tumor control.

Loss of TIGIT expression also enhanced CAR-NK proliferation and persistence within the solid TiME. Persistence and proliferation were key factors for antitumor activity and objective responses in patients in two recent adoptive CAR-NK clinical trials against hematologic malignancies (4, 5). In solid tumors, which contain TiMEs that would result in impaired proliferation of infiltrating NK cells, enhancement of CAR-NK proliferation is likely more critical to ensure adequate antitumor activity (46). We observed reduced CAR-NK proliferation in the presence of a TIGIT ligand–enriched TiME that was rescued by deletion of TIGIT. This can be explained by the fact that TIGIT typically suppresses the NF-κβ signaling responsible for CAR-induced NK proliferation (10, 47). Indeed, this is supported by our data showing that TIGIT deletion improved proliferation and persistence of CAR-modified but not unmodified NK cells in the TiME. It is also possible that the improved persistence observed with TIGIT loss in CAR-NKs is due to decreased proapoptotic signaling. We observed that TIGIT^{KO}GD2.CAR-NKs after tumor exposure had decreased expression of the proapoptotic gene *BID* and *PDCD2*. This suggests that TIGIT may inhibit CAR-NK persistence by directly promoting *BID* transcription or by interfering with upstream negative regulators of BID including AKT, thus leading to impaired long-term persistence in the TiME (48, 49). Loss of TIGIT can possibly reverse this process, analogous to the way that PD-1 blockade can improve the persistence of CAR-T cells by reducing the upregulation of Fas receptor and proapoptotic genes induced after CAR-mediated activation (48, 50–52).

In summary, we defined a unique role for TIGIT in genetically engineered human CAR-NKs. We have shown that generation of a *TIGIT*-deleted CAR-NK product is achievable and that TIGIT^{KO}-GD2.CAR-NKs exhibit antitumor activity, expand, and persist within a TIGIT ligand–enriched suppressive solid tumor microenvironment. Our CAR-NK manufacturing protocol incorporating TIGIT deletion via CRISPR/Cas9 can be broadly applied to human NK cell products expressing any solid tumor CAR. Experiments investigating the antitumor effect of TIGIT deletion in numerous CAR antigen and tumor contexts *in vivo* are needed to more broadly apply our findings and are ongoing. We demonstrated that traditional inhibitory TIGIT signaling does not play a vital role in the context of CARs and does not account for the improved CAR activity observed in our study. Instead, we highlight a noncanonical role for TIGIT in modulating cell adhesion and immune synapse strength in CAR-NKs within TIGIT ligand–enriched TiMEs. These findings will hopefully guide new biology-driven strategies to overcome inhibitory NK receptors like TIGIT and improve the efficacy of CAR-NKs against solid tumors.

Authors' Disclosures

N. Varadarajan reports grants from Cancer Prevention and Research Institution of Texas and NIH during the conduct of the study; other support from AuraVax Therapeutics and CellChorus outside the submitted work; a patent 11774449 issued and licensed to CellChorus; and being a co-founder of CellChorus and AuraVax Therapeutics. No disclosures were reported by the other authors.

Authors' Contributions

I. Navin: Data curation, formal analysis, validation, investigation, visualization, methodology, writing–original draft, writing–review and editing. **M. Dysthe:** Data curation, validation, visualization, methodology. **P.S. Menon:** Resources, data curation, formal analysis, investigation, methodology, writing–review and editing. **C. Baumgartner:** Validation, investigation. **T. Sauer:** Conceptualization. **N. Varadarajan:** Resources, data curation, supervision, investigation, methodology, writing–review and editing. **R. Parihar:** Conceptualization, resources, data curation, supervision, funding acquisition, investigation, writing–review and editing.

Acknowledgments

R. Parihar was supported by an Alex's Lemonade Stand Foundation A Award and the American Cancer Society Mission Boost Grant. N. Varadarajan acknowledges support from the NIH (R01GM143243) and Cancer Prevention and Research Institution of Texas (RP240439).

Note

Supplementary data for this article are available at Cancer Immunology Research Online (http://cancerimmunolres.aacrjournals.org/).

Received September 19, 2024; revised February 19, 2025; accepted July 25, 2025; posted first July 29, 2025.

References

1. Sivori S, Vacca P, Del Zotto G, Munari E, Mingari MC, Moretta L. Human NK cells: surface receptors, inhibitory checkpoints, and translational applications. Cell Mol Immunol 2019;16:430–41.
2. Miller JS, Soignier Y, Panoskaltsis-Mortari A, McNearney SA, Yun GH, Fautsch SK, et al. Successful adoptive transfer and in vivo expansion of human haploidentical NK cells in patients with cancer. Blood 2005;105:3051–7.
3. Pfeiffer T, Zimmerman C, Berrien-Elliott MM, Foltz J, Becker-Hapak M, Neal C, et al. Donor-derived memory-like NK cells for the treatment of children and young adults with relapsed AML following allo-HCT. Transpl Cell Ther 2024;30:S12.
4. Liu E, Marin D, Banerjee P, Macapinlac HA, Thompson P, Basar R, et al. Use of CAR-transduced natural killer cells in CD19-positive lymphoid tumors. N Engl J Med 2020;382:545–53.
5. Marin D, Li Y, Basar R, Rafei H, Daher M, Dou J, et al. Safety, efficacy and determinants of response of allogeneic CD19-specific CAR-NK cells in CD19+ B cell tumors: a phase 1/2 trial. Nat Med 2024;30:772–84.
6. Ephraim R, Fraser S, Nurgali K, Apostolopoulos V. Checkpoint markers and tumor microenvironment: what do we know? Cancers 2022;14:3788.
7. Wen J, Mao X, Cheng Q, Liu Z, Liu F. A pan-cancer analysis revealing the role of TIGIT in tumor microenvironment. Sci Rep 2021;11:22502.
8. Bevelacqua V, Bevelacqua Y, Candido S, Skarmoutsou E, Amoroso A, Guarneri C, et al. Nectin like-5 overexpression correlates with the malignant phenotype in cutaneous melanoma. Oncotarget 2012;3:882–92.
9. Molfetta R, Zitti B, Lecce M, Milito ND, Stabile H, Fionda C, et al. CD155: a multi-functional molecule in tumor progression. Int J Mol Sci 2020;21:922.
10. Li M, Xia P, Du Y, Liu S, Huang G, Chen J, et al. T-Cell immunoglobulin and ITIM domain (TIGIT) receptor/poliovirus receptor (PVR) ligand engagement suppresses interferon-γ production of natural killer cells via β-arrestin 2-mediated negative signaling. J Biol Chem 2014;289:17647–57.
11. Bi J, Zhang Q, Liang D, Xiong L, Wei H, Sun R, et al. T-cell Ig and ITIM domain regulates natural killer cell activation in murine acute viral hepatitis. Hepatol Baltim Md 2014;59:1715–25.

12. Bi J, Zheng X, Chen Y, Wei H, Sun R, Tian Z. TIGIT safeguards liver regeneration through regulating natural killer cell-hepatocyte crosstalk. Hepatol Baltim Md 2014;60:1389–98.
13. Heczey A, Liu D, Tian G, Courtney AN, Wei J, Marinova E, et al. Invariant NKT cells with chimeric antigen receptor provide a novel platform for safe and effective cancer immunotherapy. Blood 2014;124:2824–33.
14. Pulè MA, Straathof KC, Dotti G, Heslop HE, Rooney CM, Brenner MK. A chimeric T cell antigen receptor that augments cytokine release and supports clonal expansion of primary human T cells. Mol Ther 2005;12:933–41.
15. Ahmed N, Ratnayake M, Savoldo B, Perlaky L, Dotti G, Wels WS, et al. Regression of experimental medulloblastoma following transfer of HER2-specific T cells. Cancer Res 2007;67:5957–64.
16. Kelly PF, Carrington J, Nathwani A, Vanin EF. RD114-pseudotyped oncoretroviral vectors. Biological and physical properties. Ann N Y Acad Sci 2001; 938:262–76.
17. Rossig C, Bollard CM, Nuchtern JG, Rooney CM, Brenner MK. Epstein-Barr virus-specific human T lymphocytes expressing antitumor chimeric T-cell receptors: potential for improved immunotherapy. Blood 2002;99:2009–16.
18. Gad AZ, Morris JS, Godret-Miertschin L, Montalvo MJ, Kerr SS, Berger H, et al. Molecular dynamics at immune synapse lipid rafts influence the cytolytic behavior of CAR T cells. Sci Adv 2025;11:eadq8114.
19. Huang R-S, Lai M-C, Shih H-A, Lin S. A robust platform for expansion and genome editing of primary human natural killer cells. J Exp Med 2021;218: e20201529.
20. Naeimi Kararoudi M, Dolatshad H, Trikha P, Hussain S-RA, Elmas E, Foltz JA, et al. Generation of knock-out primary and expanded human NK cells using Cas9 ribonucleoproteins. J Vis Exp 2018;136:58237.
21. Parihar R, Rivas C, Huynh M, Omer B, Lapteva N, Metelitsa LS, et al. NK cells expressing a chimeric activating receptor eliminate MDSCs and rescue impaired CAR-T cell activity against solid tumors. Cancer Immunol Res 2019;7:363–75.
22. Chockley PJ, Ibanez-Vega J, Krenciute G, Talbot LJ, Gottschalk S. Synapse-tuned CARs enhance immune cell anti-tumor activity. Nat Biotechnol 2023;41: 1434–45.
23. Liadi I, Roszik J, Romain G, Cooper LJN, Varadarajan N. Quantitative high-throughput single-cell cytotoxicity assay for T cells. J Vis Exp 2013;72:e50058.
24. Rezvan A, Romain G, Fathi M, Heeke D, Martinez-Paniagua M, An X, et al. Identification of a clinically efficacious CAR T cell subset in diffuse large B cell lymphoma by dynamic multidimensional single-cell profiling. Nat Cancer 2024;5:1010–23.
25. Lapteva N, Durett AG, Sun J, Rollins LA, Huye LL, Fang J, et al. Large-scale ex vivo expansion and characterization of natural killer cells for clinical applications. Cytotherapy 2012;14:1131–43.
26. Romee R, Schneider SE, Leong JW, Chase JM, Keppel CR, Sullivan RP, et al. Cytokine activation induces human memory-like NK cells. Blood 2012;120:4751–60.
27. Jayaraman P, Parikh F, Newton JM, Hanoteau A, Rivas C, Krupar R, et al. TGF-β1 programmed myeloid-derived suppressor cells (MDSC) acquire immune-stimulating and tumor killing activity capable of rejecting established tumors in combination with radiotherapy. Oncoimmunology 2018;7:e1490853.
28. Chen L, Wang S, Wang Y, Zhang W, Ma K, Hu C, et al. IL-6 influences the polarization of macrophages and the formation and growth of colorectal tumor. Oncotarget 2018;9:17443–54.
29. Tran HC, Wan Z, Sheard MA, Sun J, Jackson JR, Malvar J, et al. TGFβR1 blockade with galunisertib (LY2157299) enhances anti-neuroblastoma activity of the anti-GD2 antibody dinutuximab (ch14.18) with natural killer cells. Clin Cancer Res 2017;23:804–13.
30. Chauvin J-M, Ka M, Pagliano O, Menna C, Ding Q, DeBlasio R, et al. IL15 stimulation with TIGIT blockade reverses cd155-mediated NK-cell dysfunction in melanoma. Clin Cancer Res 2020;26:5520–33.
31. Zhang Q, Bi J, Zheng X, Chen Y, Wang H, Wu W, et al. Blockade of the checkpoint receptor TIGIT prevents NK cell exhaustion and elicits potent anti-tumor immunity. Nat Immunol 2018;19:723–32.
32. Lang Y, Huang H, Jiang H, Wu S, Chen Y, Xu B, et al. TIGIT blockade reshapes the tumor microenvironment based on the single-cell RNA-sequencing analysis. J Immunother 2024;47:172–81.
33. Jackson Z, Hong C, Schauner R, Dropulic B, Caimi PF, de Lima M, et al. Sequential single-cell transcriptional and protein marker profiling reveals TIGIT as a marker of CD19 CAR-T cell dysfunction in patients with non-hodgkin lymphoma. Cancer Discov 2022;12:1886–903.
34. Liu L, You X, Han S, Sun Y, Zhang J, Zhang Y. CD155/TIGIT, a novel immune checkpoint in human cancers (Review). Oncol Rep 2021;45:835–45.
35. Hasan MF, Campbell AR, Croom-Perez TJ, Oyer JL, Dieffenthaller TA, Robles-Carrillo LD, et al. Knockout of the inhibitory receptor TIGIT enhances the antitumor response of ex vivo expanded NK cells and prevents fratricide with therapeutic Fc-active TIGIT antibodies. J Immunother Cancer 2023;11: e007502.
36. He Y, Sun MM, Zhang GG, Yang J, Chen KS, Xu WW, et al. Targeting PI3K/Akt signal transduction for cancer therapy. Signal Transduct Target Ther 2021; 6:425.
37. Worboys JD, Vowell KN, Hare RK, Ambrose AR, Bertuzzi M, Conner MA, et al. TIGIT can inhibit T cell activation via ligation-induced nanoclusters, independent of CD226 co-stimulation. Nat Commun 2023;14:5016.
38. Banta KL, Xu X, Chitre AS, Au-Yeung A, Takahashi C, O'Gorman WE, et al. Mechanistic convergence of the TIGIT and PD-1 inhibitory pathways necessitates co-blockade to optimize anti-tumor $CD8^+$ T cell responses. Immunity 2022;55:512–26.e9.
39. Urlaub D, Höfer K, Müller M-L, Watzl C. LFA-1 activation in NK cells and their subsets: influence of receptors, maturation, and cytokine stimulation. J Immunol 2017;198:1944–51.
40. Briercheck EL, Trotta R, Chen L, Hartlage AS, Cole JP, Cole TD, et al. PTEN is a negative regulator of NK cell cytolytic function. J Immunol 2015;194: 1832–40.
41. Netter P, Anft M, Watzl C. Termination of the activating NK cell immunological synapse is an active and regulated process. J Immunol 2017;199: 2528–35.
42. Halim L, Das KK, Larcombe-Young D, Ajina A, Candelli A, Benjamin R, et al. Engineering of an avidity-optimized CD19-specific parallel chimeric antigen receptor that delivers dual CD28 and 4-1BB Co-stimulation. Front Immunol 2022;13:836549.
43. Greenman R, Pizem Y, Haus-Cohen M, Goor A, Horev G, Denkberg G, et al. Shaping functional avidity of CAR T cells: affinity, avidity, and antigen density that regulate response. Mol Cancer Ther 2021;20:872–84.
44. Davenport AJ, Cross RS, Watson KA, Liao Y, Shi W, Prince HM, et al. Chimeric antigen receptor T cells form nonclassical and potent immune synapses driving rapid cytotoxicity. Proc Natl Acad Sci U S A 2018;115:E2068–76.
45. Romain G, Strati P, Rezvan A, Fathi M, Bandey IN, Adolacion JRT, et al. Multidimensional single-cell analysis identifies a role for CD2-CD58 interactions in clinical antitumor T cell responses. J Clin Invest 2022;132:e159402.
46. Zhang S, Liu W, Hu B, Wang P, Lv X, Chen S, et al. Prognostic significance of tumor-infiltrating natural killer cells in solid tumors: a systematic review and meta-analysis. Front Immunol 2020;11:1242.
47. Gomes-Silva D, Mukherjee M, Srinivasan M, Krenciute G, Dakhova O, Zheng Y, et al. Tonic 4-1BB costimulation in chimeric antigen receptors impedes T cell survival and is vector dependent. Cell Rep 2017;21:17–26.
48. Gibbons RM, Liu X, Pulko V, Harrington SM, Krco CJ, Kwon ED, et al. B7-H1 limits the entry of effector CD8+ T cells to the memory pool by upregulating Bim. Oncoimmunology 2012;1:1061–73.
49. Majewski N, Nogueira V, Robey RB, Hay N. Akt inhibits apoptosis downstream of BID cleavage via a glucose-dependent mechanism involving mitochondrial hexokinases. Mol Cell Biol 2004;24:730–40.
50. Huan T, Chen D, Liu G, Zhang H, Wang X, Wu Z, et al. Activation-induced cell death in CAR-T cell therapy. Hum Cell 2022;35:441–7.
51. Gargett T, Yu W, Dotti G, Yvon ES, Christo SN, Hayball JD, et al. GD2-specific CAR T cells undergo potent activation and deletion following antigen encounter but can be protected from activation-induced cell death by PD-1 blockade. Mol Ther 2016;24:1135–49.
52. Valeri A, García-Ortiz A, Castellano E, Córdoba L, Maroto-Martín E, Encinas J, et al. Overcoming tumor resistance mechanisms in CAR-NK cell therapy. Front Immunol 2022;13:953849.